JGR Oceans

RESEARCH ARTICLE
10.1029/2018JC014576

Key Points:
- Choice of added ligand is critical in these measurements, and elucidation of the Fe-binding organic ligand pool is dependent on the use of multiple methods
- The TransPolar Drift transport high dissolved Fe (DFe) thanks to Fe-binding organic ligands (L_t)
- This L_t is predominantly humic-terrestrial derived

Supporting Information:
- Supporting Information S1

Correspondence to:
H. A. Slagter,
hans.a.slagter@outlook.com

Citation:
Slagter, H. A., Laglera, L. M., Sukekava, C., & Gerringa, L. J. A. (2019). Fe-binding organic ligands in the humic-rich TransPolar drift in the surface Arctic Ocean using multiple voltammetric methods. *Journal of Geophysical Research: Oceans*, *124*, 1491–1508. https://doi.org/10.1029/2018JC014576

Received 16 SEP 2018
Accepted 23 JAN 2019
Accepted article online 30 JAN 2019
Published online 7 MAR 2019

©2019. American Geophysical Union. All Rights Reserved.

Fe-Binding Organic Ligands in the Humic-Rich TransPolar Drift in the Surface Arctic Ocean Using Multiple Voltammetric Methods

Hans A. Slagter[1], Luis M. Laglera[2], Camila Sukekava[2], and Loes J. A. Gerringa[1]

[1]NIOZ Royal Netherlands Institute for Sea Research, Department of Ocean Systems (OCS) and Utrecht University, Den Burg, Netherlands, [2]FI-TRACE, Departamento de Química, Universidad de las Islas Baleares, Palma, Spain

Abstract Samples inside and outside the Arctic Ocean's TransPolar Drift (TPD) have been analyzed for Fe-binding organic ligands (L_t) with Competitive Ligand Exchange Adsorptive Stripping Voltammetry (CLE-AdCSV) using salicylaldoxime (SA). This analysis is compared to prior analyses with CLE-AdCSV using 2-(2-thiazolylazo)-p-cresol (TAC). The TPD's strong terrestrial influence is used to compare the performance of both CLE-AdCSV methods in representing the nature of natural organic ligands. These measurements are compared against direct voltammetric determination of humic substances (HS) and spectral properties of dissolved organic matter. The relationship between the two CLE-AdCSV derived [L_t] versus HS in the TPD has a comparable slope, with a 40% offset toward higher values obtained with SA. Higher [L_t] values inside the TPD, most probably due to HS, explain high dissolved Fe concentrations transported over the Arctic Ocean by the TPD. Outside of the TPD in the surface Arctic Ocean HS occur as well but at lower concentrations. Here changes in HS relate to changes in dissolved Fe concentration and to [L_t] obtained with SA, whereas [L_t] obtained with TAC remain constant. Moreover, with decreasing HS the offset between the methods using TAC and SA decreases. We surmise that in the presence of HS, the TAC method detects HS only either at higher concentrations or of specific composition. On the other hand, the SA method might overestimate [L_t], as an offset with the TAC method that remains constant where HS are not detected. Regardless, HS are the dominant type of Fe-binding organic ligand in the surface of the Arctic Ocean.

Plain Language Summary The Arctic Ocean is surrounded by land and is subject to strong influences of surrounding rivers. Climate change-induced increases in organic material from these rivers have already been reported, making the role of river runoff for the biogeochemistry of the open Arctic Ocean an urgent question. Water with a riverine component is carried across the Arctic Ocean via a stream of surface seawater and sea ice known as the Transpolar Drift. A component of organic material brought into the Arctic Ocean surface is humic substances, organic breakdown products from plant material known for their ability to bind iron. Iron is an essential trace element for primary production in the oceans and does not dissolve well in seawater without being bound by a dissolvable substance, of which the humic substances are an example among many. This study aims to gain insight into the role of humic substances in the binding of iron in the Arctic Ocean using multiple electrochemical methods while also discussing the suitability of these methods in the ongoing effort to characterize the diverse pool of iron binding organic substances.

1. Introduction

Fe is an essential trace metal for marine primary production (Geider & La Roche, 1994; Netz et al., 2012; Zhang, 2014). Fe solubility in seawater is governed by the presence of organic ligands binding Fe, as inorganic solubility is lower than the minimum required concentrations for primary productivity (Boyd et al., 2012; Strzepek et al., 2011; Timmermans, Davey, et al., 2001; Timmermans, Gerringa, et al., 2001; Wilhelm et al., 2013). Fe-binding organic ligands form a poorly characterized pool as part of dissolved organic matter (DOM; Gledhill, 2012; Hassler et al., 2017). Some very specific contributors such as siderophores are now becoming better characterized, though the relative contribution of these is in picomolar ranges and is a minor fraction of high dissolved Fe (DFe) and the Fe-binding organic ligand concentrations (Boiteau et al., 2016; Bundy et al., 2018; Gledhill et al., 2004; Velasquez et al., 2016, 2011). Given the inherently indirect nature of Fe-binding organic ligand measurements, the relative contribution of different

groups of Fe-binding organic ligands is as of yet unknown. However, relative contributions by groups like humic substances (HS; Laglera & van den Berg, 2009) and exopolymeric substances (Hassler et al., 2011) may be considerable. We know from a previous study on one station in the Arctic Ocean, also described in this paper, that the Fe-binding organic binding sites consist for 62% of HS (Sukekava et al., 2018).

The surface of the Arctic Ocean is strongly affected by terrestrial DOM as it is a shelf-surrounded ocean subject to terrestrial influences, with a very high source area to basin ratio as defined by Raiswell and Anderson (2005). Runoff from the many rivers contains complex organic material, which for a large part is deposited in the Arctic shelf seas (Guéguen et al., 2007). The input of terrestrial HS is thought to be a major influence in the context of Fe-binding organic ligands (Batchelli et al., 2010; Hioki et al., 2014; Krachler et al., 2015; Nakayama et al., 2011). HS are persistent and heterogeneous complex organic degradation products, ubiquitous particularly in coastal areas (Benner et al., 2005; Buffle, 1990), and have long been known to bind trace metals (Buffle, 1988). In fact, HS have been shown to account for an important part of the Fe-binding capacity in seawater (Abualhaija et al., 2015; Dulaquais et al., 2018; Laglera & van den Berg, 2009). HS are a complex black box with components that are typically operationally defined (Buffle, 1988). Humic acids are hydrophobic at low pH and therefore separated from fulvic acid by precipitation after acidification (Bronk, 2002; Buffle, 1988); these form the oldest or most recalcitrant fraction of HS. A distinction is also made between terrestrial HS and marine humic or humic-like substances, produced in situ by marine microbial activity as opposed to transported in from a terrestrial source (Bronk, 2002; Nakayama et al., 2011). However, this distinction is hypothetical and cannot be supported by analytical means. Low salinity waters in the surface Arctic Ocean carry important DOM concentrations of terrestrial nature, whereas marine humics could contribute significantly to higher salinity waters.

The definition of HS is essentially operational, based on column retention with alkaline elution (Buffle, 1990). These analytical techniques are very time consuming and hard to apply in seawater. Spectral properties of DOM (chromophoric DOM or CDOM and fluorescent DOM or FDOM) are indicative of many subgroups, including HS (Coble, 2007). Measurements of HS and their relative contribution to the Fe-binding organic ligand pool are not straightforward. Direct voltammetric measurement of HS is possible (Laglera et al., 2007; Quentel & Filella, 2008).

Measurement of Fe-binding organic ligands using Competitive Ligand Exchange-Adsorptive Cathodic Stripping Voltammetry (CLE-AdCSV) is a technique proven to resolve the presence of most major ligands in the ocean (Croot & Johansson, 2000; Gledhill & van den Berg, 1994; Rue & Bruland, 1995; van den Berg, 2006). However, elucidation of the contribution of HS has met with mixed results. Voltammetric determination of Fe-binding organic ligands measures the concentration and binding strength integrally for the Fe-binding organic ligand pool as a whole within the detection window of the competing ligand, and these are at best divided into several groups by binding strength. According to Laglera et al. (2011), the method using 2-(2-thiazolylazo)-p-cresol (TAC) as a competing ligand (Croot & Johansson, 2000) does not reflect certain HS. In contrast, recent work using salicylaldoxime (SA) as competing ligand has been shown to indicate HS (Abualhaija & van den Berg, 2014; Bundy et al., 2015; Laglera et al., 2011; Mahmood et al., 2015).

The surface of the Arctic Ocean is of particular interest due to the relatively well-constrained Transpolar Drift (TPD) surface current. It is well established that the TPD transports riverine-based water and ice from the shelf seas across the Arctic Ocean, eventually out to the Atlantic Ocean through the Fram Strait (Gordienko & Laktionov, 1969; Gregor et al., 1998). The flow path of the TPD varies yearly with the Arctic Oscillation Index (Macdonald et al., 2005) and has been constrained in the context of DOM and Fe biogeochemistry (Rijkenberg et al., 2018; Slagter et al., 2017). Given its susceptibility to rapid climate change (Intergovernmental Panel on Climate Change, 2014), the Arctic Ocean is a particularly important region to study the biogeochemistry of terrestrial matter. A rapid increase in widespread loss of permafrost (Schuur et al., 2015) will increase the deposition of terrestrial organic matter in the Arctic shelf seas (Vonk et al., 2013). The effects on the larger Arctic Ocean are still largely unknown.

Here we study a selection of samples from the ice-covered center of the Arctic Ocean and one of its open shelf seas. Samples were collected during the 2015 PS94 TransArcII expedition. Samples from inside the TPD are subject to terrestrial influence from major Arctic rivers (Rutgers van der Loeff et al., 2012), while for samples from outside the TPD and in the Barents Sea the major influence is from the shelf and Atlantic inflow (Rudels, 2012). Prior in situ measurements of HS and CDOM established that the TPD carries HS, though

they were also detected in nontrivial concentrations outside of the TPD flow path (Slagter et al., 2017), which is unsurprising as HS and/or marine humics are ubiquitous also in noncoastal waters (Obernosterer & Herndl, 2000).

Slagter et al. (2017) reported a strong relation between Fe-binding organic ligand measurements and the TPD. The study found increased [L_t] and humic representative CDOM and FDOM in the surface Arctic Ocean where the TPD is present. The prior study used TAC as a competing ligand in CLE-AdCSV; the present study expands on this by reanalyzing selected samples using SA as a competing ligand, as well as performing additional direct voltammetric measurements of HS. Comparing these results with those using TAC, we provide an explanation to the values of ligand concentration below dissolved iron concentrations found in Slagter et al. (2017). This serves to explain the elevated concentrations of DFe entering the Arctic Ocean, transported across it by the TPD and ultimately introduced into the North Atlantic Ocean. It is essential to elucidate this pathway for DFe, which supports primary production in the rapidly changing Arctic. Both the introduction of DFe bound by organic material and the availability of surface water unimpeded by ice cover are expected to increase. We hope to confirm limitations in the measurement of natural ligands, which have the potential to be electroactive such as HS, and to further unveil the relative contribution of HS in the Fe-binding organic ligand pool in the Arctic Ocean, the TPD, and in the coastal Barents Sea.

2. Materials and Methods

All data are given in Tables S1 and S2 in the supporting information.

2.1. Sampling and Sample Conservation

Specific samples collected during the 2015 PS94 TransArcII expedition onboard FS Polarstern were analyzed with the TAC method (Slagter et al., 2017). Samples were frozen at −20 °C when analysis was not done within 5 days. For the TAC method stations 69, 99, and 125 were analyzed onboard, while stations 101 and 153 were analyzed in the home laboratory in February and March 2016. After thawing and sampling for TAC, the samples were immediately frozen again. For the SA method all samples were stored at −20 °C and analyzed in the home laboratory from the same sample bottles as used for TAC, with the exception of station 99, which was sampled in duplicate. Analysis of samples with the SA method was performed in April 2017 on 47 samples at stations 69, 99, 101, 125, and 153 (Figure 1) together with one or two TAC analyses per station, checking conservation effects.

Stations 69 and 125 are full depth profiles in the open Arctic Ocean (3,500 and 4,200 m, respectively), station 153 is a full depth profile over the Barents Sea shelf (400 m), and stations 99 and 101 have been sampled for the top 200 m.

2.2. Voltammetric Determination of Fe-Binding Organic Ligands

2.2.1. TAC

For the TAC method (Croot & Johansson, 2000) a natural sample was left to equilibrate with TAC in the presence of a mixed boric acid-ammonia buffer (1M, pH 8.05, Merck) and increasing standard additions of Fe (III). Cups of 30-ml PTFE (Savillex) were used to equilibrate 10-ml subsamples from a mix of natural sample, buffer (5-mM final concentration) and TAC (10-μM final concentration) with discrete Fe (III) additions of 0 (twice), 0.2, 0.4, 0.6, 0.8, 1.0, 1.2, 1.5, 2.0, 2.5, 3.0, 4.2, 6.0, and 8.1 (twice) nM. Equilibration lasted a minimum of 8 hr to overnight.

TAC (Alfa Aesar) was dissolved in three times distilled (3xD-) methanol to a stock concentration of 0.02 M; Fe standards (1 and 3×10^{-6} M) were prepared in MQ from a 1,000-ppm ICP stock solution (Fluka) and acidified using 2xD-HNO_3. The voltammetric apparatus consisted of a 663 VA stand (Metrohm) equipped with a Hg drop multimode electrode with silanized capillary, double-junction Ag/AgCl reference electrode (KCl 3 M) and glassy carbon auxiliary electrode in a polytetrafluoroethylene cell (all Metrohm), control hardware (μAutolab III, Metrohm Autolab B.V.), and a consumer laptop PC running Nova 1.9 (Metrohm Autolab B.V.). N_2 was used for purging and Hg drop formation. When measurements were performed at sea, interference from ship motion and vibration was minimized by suspending the VA stand in elastic bands. Any electrical interference was minimized using a consumer inline peak filter and an uninterruptible power supply with sinewave converter (Fortress 750, Best Power). Analysis was performed using a slightly altered version of the measurement procedure used by Croot and Johansson (2000): Purging for 180 s, no conditioning,

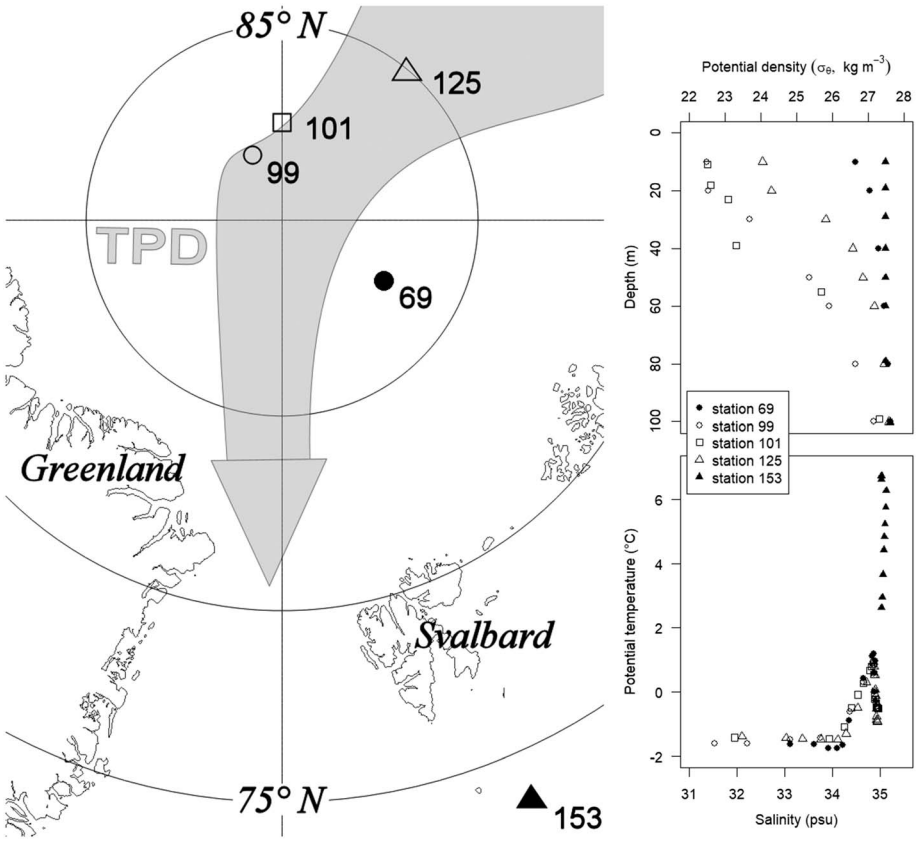

Figure 1. Map of the study area showing the selected stations 69, 99, 101, 125, and 153. The expected flow path of the TPD after Slagter et al. (2017) is shown by the gray arrow. Potential density (top right) is shown for the upper 100 m indicating the TPD influence. A potential temperature-salinity (Θ-S) plot of the selected stations is shown to the lower right. TPD = TransPolar Drift.

deposition for 140 s at −0.4 V, a 5-s equilibration followed by a differential pulse scan from −0.4 to −0.9 V. The influence of high-frequency vibrations from the ship's drivetrain was minimized by an increased scan rate of 80 mV/s, resulting from a modulation time of 4 ms and an interval time of 50 ms.

2.2.2. SA

We used a mix of procedures with SA as competing ligand as described by Buck et al. (2007, 2012) and Abualhaija and van den Berg (2014). Specifically, we adapted the pH to pH = 8.4 to acquire sufficient peak separation on our system (Buck et al., 2007 used pH = 8.2; Abualhaija et al., 2015 used pH = 8.18) and adopted the equilibration time according to Buck et al. (2007). The voltammetric apparatus, as described above for TAC, was modified to purge with synthetic air (Abualhaija & van den Berg, 2014) while still using nitrogen pressure for mercury drop formation. Nitrogen leakage in the cell was checked and did not occur. We used 25-μM SA as final concentration (Buck et al., 2007), prepared from a stock solution prepared in 3xD-methanol.

The samples were left to equilibrate with Fe (III) additions as described for TAC for 1 hr prior to measurement of the first subsample. The 25-μM SA was added 15 min prior to measurement for each subsample according to the procedure of Buck et al. (2007). To confirm the timing of the SA addition, experiments were performed following the formation of the FeSA peak with time, studying the FeSA-$FeSA_2$ kinetics as described by Abualhaija and van den Berg (2014). We observed a consistent plateau of constant peak height during 20–30 min after an initial fast rise. We assumed that FeSA was the dominant species at this time and the decline in peak height we attributed to the formation of the not electroactive species $FeSA_2$. SA analysis settings were a variation of those used by Abualhaija and van den Berg (2014). Deposition time was 240 s at 0 V followed by a differential pulse sweep from 0 to −0.7 V with a modulation time of 4 ms, an interval time of 100 ms, a step potential of 6 mV, and 50-mV modulation amplitude, resulting in a 60-mV/s scan rate.

2.3. Calculation of Organic Ligand Parameters

Titration results were fitted to a nonlinear Langmuir model (Gerringa et al., 2014), with modes for a single ligand class (L_t) and two ligand classes (L_1 and L_2) using R (R Development Core Team, 2008). DFe concentrations used in these calculations were derived from Flow Injection Analysis measurements (Rijkenberg et al., 2018) either from parallel samples onboard (stations 69, 99, and 125) or from the frozen samples in the home lab (stations 101 and 153). The Langmuir model yields the ligand concentration ($[L_t]$ or $[L_1] + [L_2]$) in equivalent nanomole of Fe (Eq. nM Fe) and the conditional stability coefficient (K' or K_1' and K_2') relative to the free Fe concentration (Fe′, which is the sum of Fe^{3+} and inorganically bound Fe) expressed as their base-10 logarithm ($\log K'_{Fe'L}$). Standard errors are included; in the case of $\log K'$ the upper and lower limits for these are reported separately.

The conditional binding strength of the added ligand (AL) is given by the K'_{FeAL} or $\beta'_{Fe(AL)2}$ in the case of bidentate association. The center of the detection window (D) is then given by the product of K'_{AL} and the free AL concentration, hence given as $D_{AL} = K'_{AL}\,[AL']$. For the Langmuir fit of the TAC data a $\log\beta_{(Fe'TAC)2}$ of 12.4 was used after Croot and Johansson (2000). For the TAC method D is given by $D_{TAC} = [TAC]^2\,\beta_{(FeTAC)2} = 251.2$. The natural logarithm of the inorganic side reaction coefficient ($\log\alpha_i$) used in the calculations for TAC at a pH of 8.05 was 10.0 (Liu & Millero, 2002; Sunda & Huntsman, 2003). For the Langmuir fit of the SA data a $\log\beta'_{Fe(SA)2}$ of 10.72 and $\log K'_{FeSA}$ of 6.52 were used, with the detection window given by $D_{SA} = (K'_{FeSA}\,[SA]) + (\beta'_{Fe(SA)2}\,[SA]^2) = 115.6$ (Abualhaija & van den Berg, 2014); the pH of 8.4 resulted in $\log\alpha_i = 10.8$ using stability constants from Millero (1998) and Liu and Millero (2002). A calibration executed with DTPA at the conditions of our measurement (15-min equilibration with [SA] = 25 μM at pH = 8.4) gave comparable K'_{FeSA} and $\beta'_{Fe(SA)2}$ ($\log K'_{FeSA} = 6.4$, $\log\beta'_{Fe(SA)2} = 11.04$, unpublished results). Although according to Abualhaija and van den Berg (2014) only FeSA is electroactive, the sum of both alphas (FeSA and $Fe(SA)_2$) is taken into account together with the inorganic side reaction coefficient α_i to calculate [Fe′], thus subtracting the contribution of the nonelectroactive $Fe(SA)_2$ from the signal.

The difference in detection window between the TAC and SA method (251.2 vs. 115.6 as log values 2.4 vs. 2.1) is not large; assuming that the detection window is 1 order of magnitude above and below the center of the window (Apte et al., 1988; Gerringa et al., 2014; van den Berg et al., 1990), the windows overlap substantially. The difference in pH between the TAC and SA method was substantial, and therefore, a correction in the inorganic side reaction coefficient α_i was necessary as described above. The resulting $[L_t]$ or $[L_1] + [L_2]$ together with stability constants K' or K_1' and K_2' was used for iterative calculations of the Fe speciation equilibrium with Newton's algorithm (Press et al., 2007), also using R (Gerringa et al., 2014; Slagter et al., 2017). These calculations yield the excess ligand concentration ([L′]) and the reactivity of the natural ligands ($\alpha'_{Fe'L} = K'\,[L']$, expressed as the base-10 logarithm, $\log\alpha'_{Fe'L}$).

2.4. Voltammetric Analysis of HS

Direct voltammetric measurement of HS was performed onboard with the same voltammetric equipment as above (after Laglera et al., 2007). Samples were buffered as for the TAC CLE-AdCSV method and saturated with Fe (III) (30 nM). $KBrO_3$ was used as an oxidizer to boost the dissociation current of the Fe-HS complex, added to a final concentration of 13 μM. Additions of 0.1- to 0.4-mg/L fulvic acid (Suwannee River Fulvic Acid Standard I, International Humic Substances Society batch number SRFA 1S101F, further referred to as SRFA) were used as a calibration standard. Therefore, HS are expressed as milligrams of SRFA per liter. The voltammetric procedure used a 3-min purge with nitrogen followed by a 90-s deposition interval at −0.1 V followed by a linear current sweep to −1.1 V at 100 mV/s.

A subset of separately filled bottles stored frozen until analysis in the laboratories of the University of the Balearic Islands (UIB lab) was analyzed after the cruise with a voltammetric system identical to the system used onboard. In this case the original voltammetric method (Laglera et al., 2007) was slightly modified to ensure the saturation with iron of the HS binding groups of both the sample and the reference standard (Sukekava et al., 2018). In the presence of 20-nM $KBrO_3$ and 5-mM POPSO buffer (from a mixed solution cleaned with MnO_2 as in Laglera et al., 2013) the sample was saturated with iron (20–60 nM depending on the DFe concentration) and was continually measured until the voltammetric signal decreased to a constant value. This decrease is caused by the total precipitation of iron in excess of the binding capacity of the HS. This process was described in Laglera and van den Berg (2009). Calibration was attained via additions of

0.2 mg of SRFA per liter, dissolved in ultrapure water and in this case carefully saturated with iron before use. HS were therefore expressed as milligrams of SRFA per liter. The data sets for [HS] from both labs (on board and UIB lab) showed good correlation and could therefore safely be combined into one (Sukekava et al., 2018) and are from here on reported after conversion to $[L_t]_{HS}$ for most purposes. A complexing capacity of 14.6 ± 0.7 mg of SRFA per liter measured using the same batch of SRFA by Sukekava et al. (2018) was used to convert HS concentrations into HS derived ligand concentrations ($[L_t]_{HS}$). The complexing capacity was obtained by titration with iron of the SRFA standard dissolved in UV-digested seawater as suggested by Laglera and van den Berg (2009).

The extent of the TPD was defined by Slagter et al. (2017) by in situ FDOM of yellow substance or HS (Rabe et al., 2016; further referred to as $FDOM_{HS}$). A surface increase of $FDOM_{HS}$ from the in situ sensor on the rosette sampler was observed where the TPD was expected. Based on this known tracer for the terrestrial influence that defines the TPD (Amon et al., 2003; Coble, 2007), the TPD influence area during our study was operationally constrained as those records where $FDOM_{HS}$ was 0.5 a.u. or higher. This threshold value is used again for the present study to define the vertical and horizontal boundary of the TPD.

3. Results

3.1. Overall Oceanographic Characteristics

The vertical and horizontal TPD influence areas in the Arctic Ocean surface coincide with a low density anomaly resulting from low surface salinity within the upper 100 m. Specifically, surface samples from stations 99, 101, and 125 inside the TPD show this low surface salinity and density (Figure 1, open symbols), down to 28 psu and 23 kg/m^3, respectively. Station 69, which is completely outside the TPD, has a higher surface salinity and density of 33.5 psu and 27 kg/m^3, respectively. Station 153 in the Barents Sea has a salinity of >35 psu and relatively constant density between 27.5 and 28 kg/m^3 with a higher potential temperature (3–7 °C; Figure 1). From the three stations having the TPD in the surface layer, station 101 is a transition station on the border of the TPD; here terrestrial influences are less well defined (Slagter et al., 2017) and the TPD occurs deeper and over a narrower band of depths as per our $FDOM_{HS}$ boundary (Figures 2b and 2e).

3.2. Arctic Fe Speciation

All SA measurements show higher $[L_t]$ than TAC measurements (Figures 2a–2c and 3a and 3b and Excess L in Figure 3b). Specifically, $[L_t]_{TAC}$ is on average 60% of $[L_t]_{SA}$ across all samples (SD = 12.9%, $N = 47$). At depths beyond 150 m $[L_t]_{SA}$ approaches the $[L_t]_{TAC}$ more closely. The difference is most pronounced for measurements inside the TPD. $[L_t]_{TAC}$ inside the TPD was in some cases lower than DFe (stations 99 and 125; Figures 2d and 2f), with more occurrences in the complete TAC data set (Slagter et al., 2017). This was not the case for $[L_t]_{SA}$, which was higher than DFe in all samples measured. Overall, $[L_t]_{TAC}$ was 2.46 ± 0.6 Eq. nM Fe inside the TPD and 1.36 ± 0.3 Eq. nM Fe outside the TPD; $[L_t]_{SA}$ was 4.19 ± 0.7 and 2.33 ± 0.6 Eq. nM Fe, respectively (Table 1). In contrast to TAC data, most SA analyses could also be resolved for two ligand groups inside the TPD. When comparing the sum of SA-derived $[L_1]$ and $[L_2]$ from the two ligand models ($\Sigma_{L1,L2;SA}$) to $[L_t]_{SA}$ from the model assuming the existence of one ligand, there is very good agreement (Figures 2a–2c and 3a and 3b). Additionally, the SA-derived $[L_1]$ has a good agreement with $[L_t]_{TAC}$ (Pearson's product-moment correlation score of 0.82 ($p < 0.001$; $N = 12$). For those samples where two ligand groups could be resolved for the TAC method, $\Sigma_{L1,L2;TAC}$ is higher than $[L_t]_{TAC}$. High surface $[L_t]_{HS}$ was especially pronounced in the upper 50 m by definition in the TPD (stations 99 and 125) with $[L_t]_{HS}$ over 4 Eq. nM Fe, coinciding with high values of parameters describing CDOM (Slagter et al., 2017). $[L_t]_{HS}$ was elevated to a lesser extent in the upper 50 m in the TPD bordering stations 101 and 69 outside the TPD (1.63 and 1.83 Eq. nM Fe, respectively), and no elevated concentrations were observed for station 153 in the Barents Sea (maximum of 1.22 Eq. nM Fe in the upper 50 m; see also Table 1 and Figures 3b and 3d). The difference between measurements of $[L_t]$ using TAC and SA ($[L_t]_{SA} - [L_t]_{TAC}$) is referred to as δLt. δLt was consistently >0 with a value inside the TPD of 1.73 ± 0.6 Eq. nM Fe, whereas outside the TPD and over the continental shelf outside the TPD flow path δLt is lower but still considerable at 0.92 ± 0.4 and 0.81 ± 0.4 Eq. nM Fe, (Table 1; ranges given are standard deviations).

$LogK'_{Fe'L}$ is similar for either method and remarkably stable (Table 1). Measurements using TAC have a $logK'_{Fe'L}$ of 12.0 ± 0.4 inside the TPD and 12.1 ± 0.2 outside the TPD. Measurements using SA have a

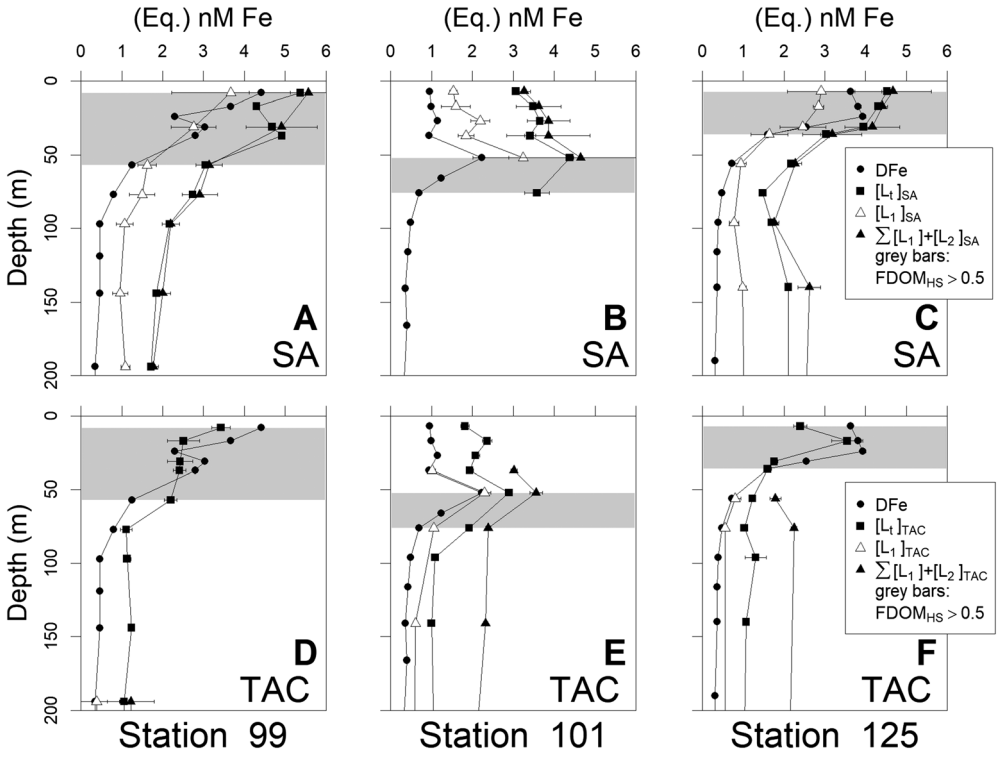

Figure 2. DFe and ligand concentrations for stations inside the TransPolar Drift influence area for determinations using a one-ligand model ($[L_t]$) and a two-ligand model ($[L_1]$ and $[L_2]$). Per station results are plotted for SA (a–c) and for TAC (d–f). The TransPolar Drift influence as determined by the $FDOM_{HS} \leq 0.5$ a.u. threshold is indicated with a gray bar. SA = salicylaldoxime; DFe = dissolved Fe; FDOM = fluorescent DOM; TAC = 2-(2-thiazolylazo)-p-cresol.

$\log K'_{Fe'L}$ of 11.8 ± 0.4 inside the TPD and 11.6 ± 0.3 outside the TPD. In the Barents Sea, $\log K'_{Fe'L}$ using TAC is similar to the other subsets at 12.1 ± 0.2, whereas here the SA method results in a lower $\log K'_{Fe'L}$ of 11.2 ± 0.2. Figure 4 shows the relation between the TAC and SA methods in terms of $\log\alpha'_{Fe'L}$, and excess L. $\log\alpha'_{Fe'L}$ is less prone to bias and therefore a good parameter for comparison (Gledhill & Gerringa, 2017). For the SA method $\log\alpha'_{Fe'L}$ is invariably near 3; for the TAC method $\log\alpha'_{Fe'L}$ is near 3 outside the TPD; inside the TPD values decrease to below 1 (Table 1 and Figure 4a). Since $\log K'_{Fe'L}$ does not significantly change inside the TPD, the low $\log\alpha'_{Fe'L}$ values for the TAC method are tied to the excess ligand concentration. Saturation of the measured ligands is indicated with excess ligands near zero and thus $\log K'_{Fe'L}$ values that are difficult to calculate. This is caused by a lack of data points with large standard deviations, thus resulting in $\log\alpha'_{Fe'L}$ values that are imprecise (Gerringa et al., 2014). This lack of performance of TAC is strongly reflected in the difference in L′, with δL′ almost twice as high inside the TPD, where L'_{TAC} is only 11% of L'_{SA}, whereas this relation is around 50% outside (Table 1). Measurements using the TAC method give consistently lower excess ligand concentrations for all depths, including sporadic occurrence of near-zero values (Figure 4b and Table 1).

While few TAC-derived measurements could resolve two ligand groups yielding few records for comparison, especially in surface samples, the $\log K'_{Fe'L}$ values for the L_1 class agree well for the TAC and SA methods (Figure S1, second column of graphs). As our TAC measurements are performed at pH = 8.05 and our SA measurements are performed at pH = 8.40, different inorganic side reaction α_i, depending on the pH, were used for the calculation of $\log K'_{Fe'L}$ making comparison possible (Gledhill, 2012). Over the entire data set $\log K_1'_{Fe'L(SA)}$ and $\log K_1'_{Fe'L(TAC)}$ do not differ significantly, with values of 13.9 ± 0.7 (N = 41) and 13.5 ± 0.6 (N = 26), respectively. The weaker L_2 class is significantly stronger in the case of TAC measurements, with an average $\log K_2'_{Fe'L,(SA)}$ of 10.4 ± 0.2 and an average $\log K_2'_{Fe'L(TAC)}$ of 11.2 ± 0.2. We cannot rule out that this difference might be due to the higher pH in the SA method because had K′ been reported in relation to Fe^{3+}, a difference does not exist. $\log\alpha'_{Fe'L}$ (Figure S1, third column) is higher toward the surface for the SA-derived L_1 fraction.

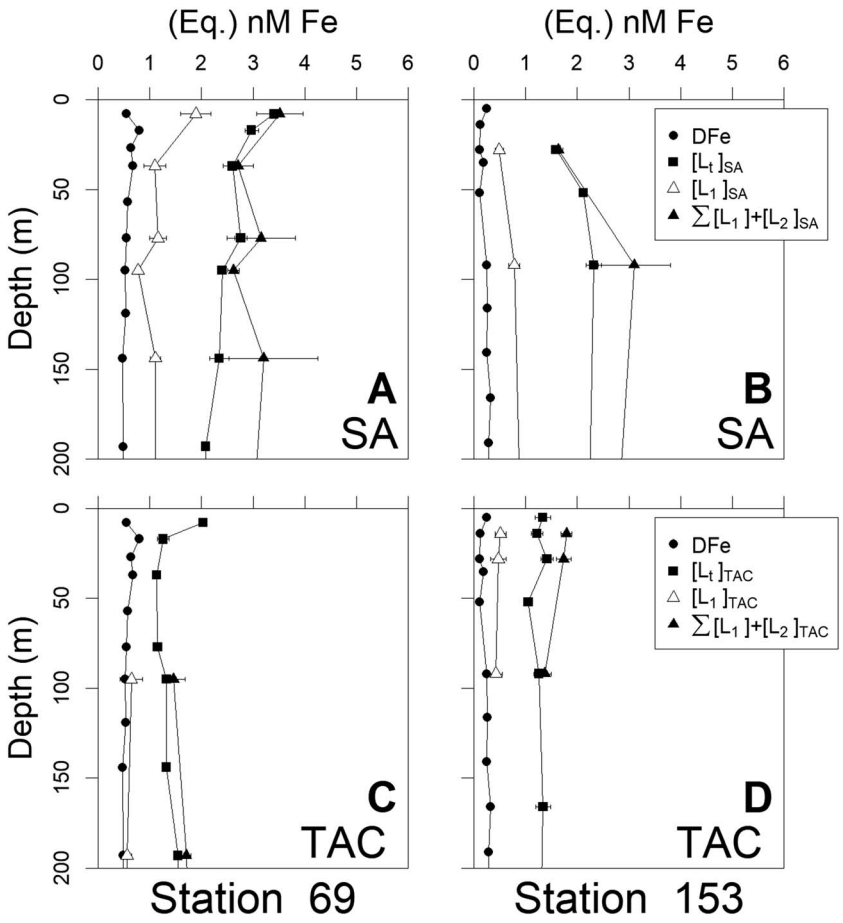

Figure 3. DFe and ligand concentrations for stations outside the TransPolar Drift influence area for determinations using a one-ligand model ($[L_t]$) and a two-ligand model ($[L_1]$ and $[L_2]$). Per station results are plotted for SA (a, b), and for TAC (c, d). SA = salicylaldoxime; DFe = dissolved Fe; TAC = 2-(2-thiazolylazo)-p-cresol.

Over the Barents Sea shelf (station 153), values are very similar regardless of the CLE-AdCSV method employed.

3.3. Method Intercomparison

When comparing $[L_t]$ between the TAC and SA methods directly, the initial view is a reasonable agreement with consistently higher values for $[L_t]_{SA}$ as noted in the prior paragraphs. All points are below the 1:1 line in favor of $[L_t]_{SA}$ (Figure 5). When we separate the data using the $FDOM_{HS} \leq 0.5$ a.u. threshold, dividing samples inside and outside the TPD, the CLE-AdCSV methods show distinct relationship with one outlier, the uppermost sample of station 69 (10-m depth; triangle in Figure 5). This outlier does not lie in the TPD according to $FDOM_{HS}$ but has elevated $[L_t]$ compared to the other values for stations outside the TPD (open circles in Figure 5). This is possibly due to a nonhumic local influence such as microbial activity but as such cannot be deemed due to HS. The relationship between $[L_t]_{TAC}$ and $[L_t]_{SA}$ at station 101 indicates that this station is in the TPD influence zone (cross symbols in Figure 5). Samples inside the TPD correlate with a slope of 0.56 ($[L_t]_{TAC}$:$[L_t]_{SA}$), whereas outside the TPD there is no correlation, with $[L_t]_{TAC}$ unchanging while $[L_t]_{SA}$ varies twofold between samples.

$LogK'_{Fe'L}$ for the measurements using SA were lower than those for the measurements using TAC, but otherwise shared a remarkable consistency, observed earlier for this data set (Slagter et al., 2017). The only exception herein is the Barents Sea station, where the difference between TAC- and SA-derived $logK'_{Fe'L}$ was slightly higher due to lower $logK'_{Fe'L}$ for measurements using SA. $Log\alpha'_{Fe'L}$ for the SA analyses does not significantly differ inside and outside the TPD. In contrast, $log\alpha'_{Fe'L}$ for TAC analyses is significantly lower inside the TPD.

Journal of Geophysical Research: Oceans

10.1029/2018JC014576

Table 1

DFe and Fe-Binding Organic Ligand Characteristics Using a 1-Ligand-Class Model for Calculation Using Both the TAC and SA Methods of CLE-AdCSV for Samples From Stations 69–125 Separated by TPD Presence Based on $FDOM_{HS} \leq 0.5$ a.u. and for Samples From Station 153 in the Barents Sea Separately

Subdivision	Statistic	DFe (nM)	$[L_t]_{TAC}$ (Eq. nM Fe)	$[L_t]_{SA}$ (Eq. nM Fe)	δL_t (Eq. nM Fe)	$[L_t]_{TAC}/[L_t]_{SA}$ (%)	Eq. nM Fe	$\log K'_{Fe'L}$ (TAC)	$\log K'_{Fe'L}$ (SA)	L'_{TAC} (Eq. nM Fe)	Eq. nM Fe	Eq. nM Fe	L'_{TAC}/L'_{SA} (%)	$\log\alpha'_{Fe'L}$ (TAC)	$\log\alpha'_{Fe'L}$ (SA)
Inside TPD	Mean	2.7	2.46	4.19	1.73	59	2.83	12	11.7	0.27	2.05	1.78	11	1.38	3.05
$FDOM_{HS} \geq 0.5$ a.u.	SD	1.17	0.6	0.7	0.6	11	1.0	0.4	0.4	0.5	0.4	0.4	19	1.2	0.3
Stations 99, 101, and 125	*N*	11	11	11	11	11	11	11	11	11	11	11	11	11	11
	Min	0.69	1.6	3.03	0.76	45	1.3	11.5	10.9	0	1.41	1.05	0.03	0.29	2.35
	Max	4.42	3.55	5.37	2.51	82	4.22	12.6	12.3	1.23	2.88	2.46	47.55	3.45	3.59
Outside TPD	Mean	0.5	1.36	2.33	0.92	62	1.04	12.1	11.6	0.86	1.77	0.94	50	3.04	2.84
$FDOM_{HS} < 0.5$ a.u.	SD	0.22	0.3	0.6	0.4	13	0.5	0.2	0.3	0.3	0.4	0.5	19	0.3	0.3
Stations 69, 99, 101, and 125	*N*	44	44	32	32	32	19	44	32	44	32	32	32	44	32
	Min	0.15	0.89	1.48	0.13	41	0.16	11.7	11.1	0.31	1.16	0.07	14.5	2.39	2.38
	Max	1.15	2.36	3.65	1.71	93	1.83	12.6	12.3	1.49	2.5	1.87	94.39	3.69	3.65
Barents Sea	Mean	0.31	1.26	2.04	0.81	62	0.7	12.1	11.2	0.95	1.67	0.8	51	3.07	2.38
Station 153	SD	0.31	0.1	0.3	0.4	18	0.4	0.2	0.2	0.3	0.4	0.4	28	0.2	0.2
	N	7	7	4	4	4	6	7	4	7	4	4	4	7	4
	Min	0.11	1.05	1.59	0.18	50	0.24	12	10.9	0.23	1.15	0.17	20.36	2.61	2.23
	Max	0.98	1.41	2.32	1.07	89	1.22	12.4	11.4	1.31	2.06	1.07	88.2	3.37	2.6

Note. Properties include the ligand concentration $[L_t]$ and the absolute difference in L_t between CLE-AdCSV methods (δL_t) and the fraction $[L_t]_{TAC}$ relative to $[L_t]_{SA}$, the relative complexation capacity attributed to HS determined directly through standard addition with SRFA ($[L_t]_{HS}$), the conditional binding constant relative to Fe′ ($\log K'_{Fe'L}$), the excess ligand concentration (L′), the absolute difference in L′ between CLE-AdCSV methods ($\delta L'$), the fraction L'_{TAC} relative to L'_{SA}, and the reactivity relative to Fe′ ($\log\alpha'_{Fe'L}$). SD = standard deviation; TAC = 2-(2-thiazolylazo)-p-cresol; SA = salicylaldoxime; CLE-AdCSV = Competitive Ligand Exchange Adsorptive Stripping Voltammetry; TPD = TransPolar Drift; FDOM = fluorescent DOM.

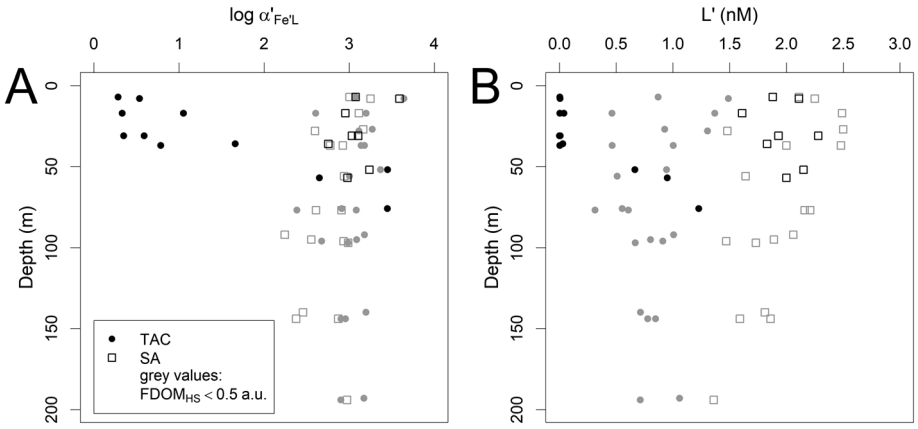

Figure 4. Log$\alpha'_{Fe'L}$ (a, dimensionless) and excess L (b, [L′] in equivalent nanomole of Fe) for the one-ligand model using TAC (closed circles) and SA (open squares) by depth. Samples outside the TPD (gray symbols) and inside the TPD (black symbols) are divided by the $FDOM_{HS} \leq 0.5$ a.u. threshold for all graphs. TAC = 2-(2-thiazolylazo)-p-cresol; SA = salicylaldoxime; FDOM = fluorescent DOM.

Differences in DFe, $[L_t]_{TAC}$, and $[L_t]_{SA}$ between samples inside and outside of the TPD were compared to differences in [HS] across the same threshold of $FDOM_{HS} \geq 0.5$. Resulting is an increment ratio between ΔDFe, $\Delta[L_t]_{TAC}$, and $\Delta[L_t]_{SA}$ over Δ[HS] (Table 2). For instance, the increment ratio for DFe may be defined as

$$\frac{\Delta DFe}{\Delta[HS]} = \frac{\overline{DFe_{inside\ TPD}} - \overline{DFe_{outside\ TPD}}}{\overline{[HS]}_{inside\ TPD} - [HS]_{outside\ TPD}} \quad (1)$$

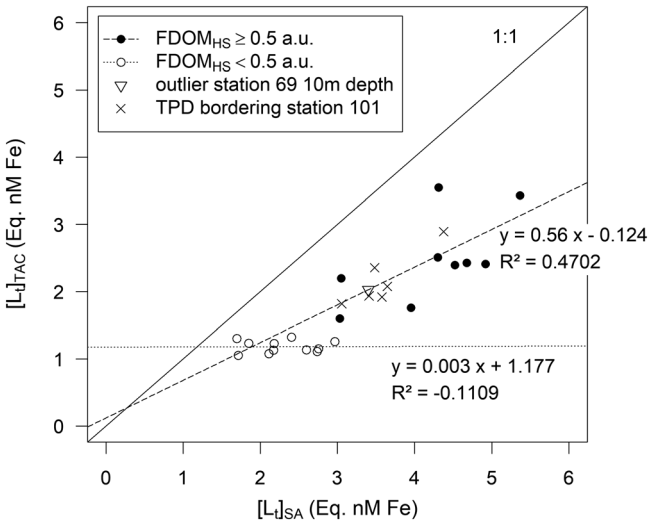

Figure 5. The ligand concentrations $[L_t]$ in equivalent nanomole of Fe as measured using Competitive Ligand Exchange Adsorptive Stripping Voltammetry with 2-(2-thiazolylazo)-p-cresol (vertical) and salicylaldoxime (horizontal) samples are subdivided on the basis of their presence inside the TPD (filled symbols, $FDOM_{HS} \geq 0.5$ a.u.) and outside the TPD (open symbols, $FDOM_{HS} < 0.5$ a.u.). One value does not conform to the split (triangle symbol), which is objectively outside the TPD influence area based on $FDOM_{HS}$; this value is not included in the regressions. Functions and R^2 values describe the linear regressions of the subsets inside and outside the TPD. Station 101, indicated by crosses, is considered inside the TPD. FDOM = fluorescent DOM; TPD = TransPolar Drift.

The $\Delta[L_t]/\Delta[HS]$ ratio is lower for TAC measurements than for SA measurements, 8.4 and 12.2 Eq. nM Fe/mg, respectively. The ΔDFe/Δ[HS] ratio is higher at 17.4 nM/mg. The lower ratio $\Delta[L_t]_{TAC}/\Delta[HS]$ indicates a lack of representation of Δ[HS] in $[L_t]_{TAC}$. However, as it is 68% of $\Delta[L_t]_{SA}/\Delta[HS]$ as opposed to near zero, some contribution to [HS] is detected by TAC. The ΔDFe/Δ[HS] and $\Delta[L_t]_{SA}/\Delta[HS]$ ratios (17.4 and 12.2, respectively) concur with the binding capacity of 14.6 ± 0.7 nM/mg found for the SRFA standard here and the value of 16.7 ± 2.0 nM/mg as found by Laglera and van den Berg (2009). This indicates that [HS] explain most DFe, $[L_t]_{SA}$ explains most HS, while $[L_t]_{TAC}$ still explains part of HS. A conversion to $[L_t]_{HS}$ has also been added in Table 2.

$[L_t]_{HS}$ and DFe have a distinct relation inside the TPD, near the 1:1 line (Figure 6a). Comparing $[L_t]_{HS}$ to TAC- and SA-derived $[L_t]$ inside the TPD (Figure 6b), both relate almost similarly though with an offset between the two comparisons (intercepts of −0.40 and 0.88 Eq. nM Fe for linear regressions of $[L_t]_{TAC}$:$[L_t]_{HS}$ and $[L_t]_{SA}$:$[L_t]_{HS}$ in Figure 6b, respectively). While $[L_t]_{TAC}$ correlates with $[L_t]_{HS}$ in a near 1:1 ratio (slope is 0.99), $[L_t]_{SA}$ has a consistently higher value while maintaining a smaller slope (0.89), confirming that $[L_t]_{SA}$ explains most HS, while $[L_t]_{TAC}$ still explains part of HS. Outside the TPD $[L_t]_{TAC}$ is constant over low but variable $[L_t]_{HS}$, whereas $[L_t]_{SA}$ and $[L_t]_{HS}$ outside the TPD covary similarly to their relation inside the TPD (gray values in Figure 6b). The lack of $[L_t]_{TAC}$ correlation with $[L_t]_{HS}$ outside the TPD corresponds to a poor correlation of $[L_t]_{HS}$ with DFe outside of the TPD (Figure 6a, gray values). Comparison between $[L_t]_{HS}$ and δL_t shows no clear correlation inside and outside of the TPD. Pearson product-moment correlation proved to

Table 2
Average Concentrations With Standard Deviations of DFe, [L_t] (Using Two CLE-AdCSV Methods) and [HS] Inside and Outside the TPD Based on $FDOM_{HS}$

	DFe (nM)	$[L_t]_{TAC}$ (Eq. nM Fe)	$[L_t]_{SA}$ (Eq. nM Fe)	[HS] (Eq. mg L^{-1})	=	Eq. $[L_t]_{HS}$ (Eq. nM Fe)
Inside TPD	2.70 ± 1.17	2.46 ± 0.63	4.19 ± 0.73	0.18 ± 0.07	=	2.63 ± 1.02
Outside TPD	0.50 ± 0.22	1.40 ± 0.42	2.64 ± 0.65	0.05 ± 0.03		0.73 ± 0.44
Δ (increment)	**2.20**	**1.06**	**1.55**	**0.13**	**=**	**1.9**
$\Delta[HS]^{-1}$	**17.4**	**8.4**	**12.2**	**1**		

Note. The increments (Δ) across the $FDOM_{HS}$ threshold (0.5 a.u.) of the averages are calculated for each property and increments divided by Δ[HS] for DFe and $[L_t]$ per mg SRFA across the TPD border. A conversion to equivalent $[L_t]_{HS}$ has been added using the conversion factor of 14.6 nM/mg after Sukekava et al. (2018). DFe = dissolved Fe; CLE-AdCSV = Competitive Ligand Exchange Adsorptive Stripping Voltammetry; HS = humic substance; TPD = TransPolar Drift; FDOM = fluorescent DOM. The bold emphasis indicates the lines most relevant to the discussion in the text. The other lines are discussed minimally or provided as reference.

be highly significant for $[L_t]_{HS}$ with DFe, with the strongest *r* values for samples inside the TPD. Similar relationships between *r* values are seen for $[L_t]_{HS}$ versus $[L_t]_{SA}$ and $[L_t]_{TAC}$, though with lower significance levels and no formal significance for the latter for samples outside of the TPD (Table 3). In contrast, the relation between $[L_t]_{HS}$ and δL_t was only significant for samples outside of the TPD, though there is a relation closer to a 1:1 ratio for the entire data set (Table 3 and Figure 6c). Paradoxically to the ratios of increment above and the occurrence of ligand saturation for measurements using TAC, the correlation score for the $[L_t]_{HS}$-$[L_t]_{TAC}$ relation inside the TPD is very similar to the $[L_t]_{HS}$-$[L_t]_{SA}$ relation.

4. Discussion

4.1. Method Justification

The two CLE-AdCSV methods were applied under different conditions that might influence the results of our comparison. Sample handling like freezing and conservation cannot be the reason for a difference in results. The TAC method was applied both to stored and frozen samples and at sea, and there was no difference in the results obtained, as also observed by (Buck et al., 2012). The difference in detection window between the TAC and SA method (251.2 vs. 115.6 or as log values 2.4 vs. 2.1) is not large. The reactivity of HS (α_{FeHS}) is close to those values (it has a maximum value of 104, $\log\alpha_{FeHS} = 2.03$; using the average $[L_t]_{HS}$ of 2.63 Eq. nM Fe from Table 2 and $\log K'_{FeHS} = 10.6$ from Laglera & van den Berg, 2009). The detection window is traditionally assumed to be 1 order of magnitude above and below the center of the detection window (Apte et al., 1988; Gerringa et al., 2014; van den Berg et al., 1990), so they overlap considerably and can

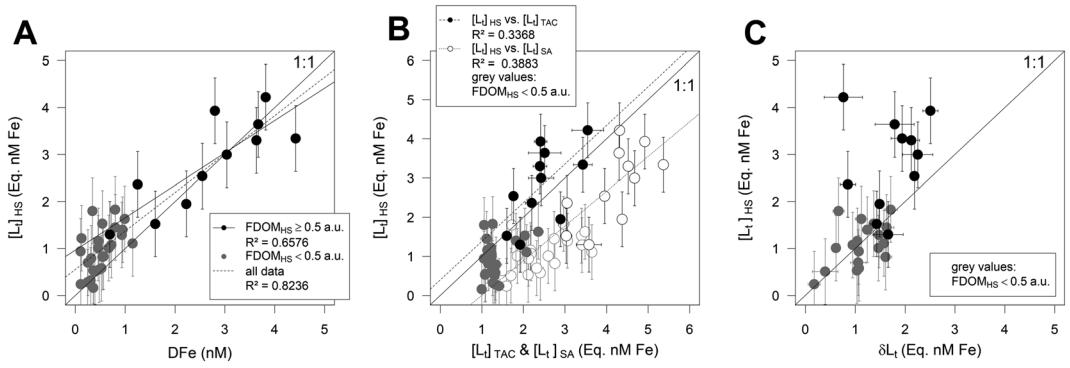

Figure 6. (a) Comparison of $[L_t]_{HS}$ and DFe. The error bars along the vertical axis are derived from the uncertainty of 0.7 nM/mg in the conversion factor from [HS] to $[L_t]_{HS}$ as determined by Sukekava et al. (2018). R^2 values indicate the quality of fit of linear regressions, of which those for all data and data inside the TransPolar Drift (TPD; $FDOM_{HS} \geq 0.5$ a.u.) are plotted. (b) Comparison of $[L_t]_{HS}$ with $[L_t]$ derived from Competitive Ligand Exchange Adsorptive Stripping Voltammetry with salicylaldoxime (open symbols) and 2-(2-thiazolylazo)-p-cresol (closed symbols). Only measurements inside the TPD ($FDOM_{HS} \geq 0.5$ a.u.) were considered for the linear regressions. (c) Comparison of $[L_t]_{HS}$ with the difference between Competitive Ligand Exchange Adsorptive Stripping Voltammetry-derived $[L_t]$ values (δLt) inside the TPD (black) and outside the TPD (gray). Gray values represent values outside of the TPD ($FDOM_{HS} < 0.5$ a.u.). DFe = dissolved Fe concentrations; FDOM = Fluorescent DOM.

Table 3
Pearson Product-Moment Correlation Scores (r) for Relationships Between $[L_t]_{HS}$ and DFe, $[L_t]$ by Two CLE-AdCSV Methods

Relation	r	*p* value		95% conf. LL	95% conf. UL
$[L_t]_{HS}$ versus DFe inside TPD	**0.83**	**0.001**	***	**0.46**	**0.96**
$[L_t]_{HS}$ versus DFe outside TPD	**0.55**	**0.004**	***	**0.20**	**0.78**
$[L_t]_{HS}$ versus $[L_t]_{TAC}$ inside TPD	0.63	0.036	*	0.06	0.89
$[L_t]_{HS}$ versus $[L_t]_{TAC}$ outside TPD	0.38	0.063		*0*	0.67
$[L_t]_{HS}$ versus $[L_t]_{SA}$ inside TPD	0.67	0.024	*	0.12	0.91
$[L_t]_{HS}$ versus $[L_t]_{SA}$ outside TPD	0.52	0.022	*	0.09	0.79
$[L_t]_{HS}$ versus δL_t inside TPD	0.17	> > 0.05		*0*	0.70
$[L_t]_{HS}$ versus δL_t outside TPD	0.49	0.031	*	0.05	0.77

Note. Lower and upper limits of 95% confidence intervals for correlations scores are reported in the last two columns. Nonoccurring $p < 0.01$ included for emphasis on significance. The italic emphasis indicates where a 0 value was forced as negative values cannot exist. DFe = dissolved Fe; CLE-AdCSV = Competitive Ligand Exchange Adsorptive Stripping Voltammetry; TPD = TransPolar Drift. The italic emphasis indicates where a 0 value was forced as negative values cannot exist. The bold emphasis indicates the lines most relevant to the discussion in the text. The other lines are discussed minimally or provided as reference.
*$p < 0.05$. **$p < 0.01$. ***$p < 0.005$.

hardly hinder in comparing the results of the two methods. We followed the method of Buck et al. (2007, 2012) in using a short equilibration time for the SA method (see section 2.2). Although we observed a steady state, we cannot be sure that equilibrium was reached between the natural ligands, SA and DFe (Laglera & Filella, 2015). This means that due to the short equilibration time, chemical labile complexes with fast dissociation rates are detected and complexes of DFe-binding organic ligands (or ligand classes) with longer dissociation rates are translated into strong ligands because SA is not able to compete during the short equilibration time. Therefore, SA possibly overestimates the ligand concentration and especially the strong ligand concentration. This might be the reason that in so many samples two ligands can be distinguished with SA, with a strong L_1 ($\log K'_{Fe'L} \geq 14$). Uncertainties are exacerbated by the fact that $FeSA_2$ has been described as nonelectroactive (Abualhaija & van den Berg, 2014). Therefore, the differences we observed might have kinetic causes. This needs further study and can render much required further insight in Fe chemistry and exchange reactions. In the present study we consequently focus on the results of the 1-ligand model for the comparison. The pH at which the SA method was applied (8.4) was higher than the pH of 8.05 used in the TAC method but was necessary to avoid peak interferences and low sensitivity. This obviously has consequences, as also described by Buck et al. (2012, 2016). They compared both methods using pH of 8 and 8.05, respectively, for the TAC method and a pH of 8.2 for the SA method. We compensated in the calculations of the ligand parameters by adapting the inorganic side reaction coefficient for Fe as described in section 2.3, and we calibrated both methods with the same artificial ligand under the specific conditions used for both methods. The calibration resulted in binding characteristics of TAC and SA very close to the published values (Abualhaija & van den Berg, 2014; Croot & Johansson, 2000). We therefore assume that a comparison is justified, but it must be kept in mind that especially kinetic differences play a role in the comparison.

With the conversion factor of 14.6 ± 0.7 nM/mg for [HS], which allows expression of equivalent nanomole of Fe per milligram (Sukekava et al., 2018), we add $[L_t]_{FA}$ as a third measure of Fe-binding organic ligands (Table 1). The conversion factor is lower than the [DFe]/[HS] increment ratio of 17.4 nM/mg (Table 2). It resembles the 16.7 ± 2.0 nM/mg as estimated by Laglera and van den Berg (2009) and the DFe/HS ratio of 13 ± 2.5 nM Fe·mg·$SRFA^{-1}$ found in Mediterranean seawater by Dulaquais et al. (2018) using a similar SRFA standard but a different analytical method (Pernet-Coudrier et al., 2013). However, we must remember that these are methodically constrained to be Fe-binding fulvic acids. In comparing the ratios of DFe and $[L_t]$ over [HS], as well as the ratios of increment going into the TPD (Table 2 and Figure 6), we find reasonable agreement with the above conversion factor in accounting for the presence of Fe in the Arctic Ocean. It may well be that the SRFA standard is too specific to describe fulvic acids as a group, but it is the best we have presently as extensively explained by Sukekava et al. (2018). The binding capacity of HS can very well have spatial and temporal differences that are currently not taken into account. Without the availability of HS standards that are specific for seawater, results need to be viewed in context of the standard used. To summarize, direct voltammetric determination of HS using SRFA correlates well with both our CLE-AdCSV

measurements, allowing explanation of at least part of the ligand pool. However, the standard will not be completely representative of material local to the Arctic Ocean.

4.2. Method Intercomparison

Overall, $[L_t]_{TAC}$ and $[L_t]_{SA}$, while both reflecting increased Fe-binding organic ligands in the TPD, are fairly different from each other. The increment ratio of 12.2 for $[L_t]_{SA}$ (Table 2) is near the complexing capacity of 14.6 ± 0.7 nM/mg found for the SRFA standard. The much lower ratio for the TAC method, 8.4 (Table 2), coincides with an underestimation relative to SA of the Fe-binding ligand pool in the TPD, which is so strongly influenced by HS. However, a very significant 61% (SD = 12.9, $N = 47$) of the $[L_t]_{SA}$ increase across the TPD boundary ($FDOM_{HS} \geq 0.5$) is still observed in $[L_t]_{TAC}$, as well as a positive increment ratio with [HS] of 68% the values for DFe and $[L_t]_{SA}$. Whereas according to Sukekava et al. (2018), on average 62% of the DFe-binding sites are from HS at station 99.

While a near 1:1 ratio is found for $[L_t]_{HS}$ versus $[L_t]_{TAC}$ (Figure 6b), $[L_t]_{HS}$ versus $[L_t]_{SA}$ gives an almost similar slope (0.89) but with a comparatively large offset. This indicates that using SA, and also outside the TPD, there are Fe-binding organic ligands which are not measured using TAC. $[L_t]_{TAC}$ does not vary with $[L_t]_{SA}$ outside the TPD (Figure 5), more or less constant $[L_t]_{TAC}$ is also observed in relation to $[L_t]_{HS}$ (Figure 6b). This further indicates that measurements with TAC do not represent all HS. Values for $[L_t]_{HS} > \delta L_t$ especially inside the TPD (Table 1 and Figure 6c) could indicate that not all unrepresented HS are accounted for by measurements using SA either. However, given the range of conversion factors reported (Laglera & van den Berg, 2009; Sukekava et al., 2018), this relation may depend on the conversion factor used. Additionally, δL_t combines two CLE-AdCSV measurements each with their own issues. The poor correlation between $[L_t]_{HS}$ and δL_t may further illustrate this (Table 3)—no single method conveys the whole picture.

Correlation of $[L_t]_{HS}$ and $[L_t]_{TAC}$ is not significant outside the TPD, and the other correlation scores of $[L_t]_{HS}$ and CLE-AdCSV-derived $[L_t]$ are of poor significance (Table 3). There is no significant correlation or poor correlation between $[L_t]_{HS}$ and δL_t inside and outside of the TPD (Figure 6c) as shown by the constant ratio $[L_t]_{TAC}/[L_t]_{SA}$ irrespective of the TPD (Table 1). This suggests that the difference between the methods is not caused by the presence of HS in the TPD alone and is indicative of a systemic difference between the CLE-AdCSV methods.

Given the limited resolution provided by the remarkably stable K′ values for either method, further characterization with CLE-AdCSV-based measurements proves difficult. In the two-ligand model $\log K'_{Fe'L}$ values were distinct between L_1 and L_2. As said above, a maximum spread of 1 order of magnitude of $\alpha'_{Fe'L}$ at each side of D_{AL} is considered to be acceptable for CLE-AdCSV measurements (Apte et al., 1988; Gerringa et al., 2014; van den Berg et al., 1990). Between L_1 and L_2 for measurements using SA, this range is close to 4 orders of magnitude (Figure S1 and Table S2b), though this is something that is not unique to the present study (Gledhill, 2012). In the present study, the upper end of the $\log K'_{Fe'L}$ interval for the L_1 class may be outside of the detection window of SA ($\log\alpha_1{}'_{Fe'L}$ of up to 5.87, whereas $\log D_{SA} = 2.06$; see also Table S2b), and thus, the large K′ range may potentially be an artifact. Moreover, due to the formation of $FeSA_2$ which is not electroactive (Abualhaija & van den Berg, 2014), the sensitivity was low at low Fe concentrations making higher K′ values more difficult to determine. Since the characteristics of both ligands are calculated simultaneously, both K′ values are influenced and may be imprecise. In the few surface samples where two ligand groups could be resolved using TAC, K_2' is nearer the detection window ($\log\alpha_1{}'_{Fe'L,TAC}$ of up to 4.5 at depths ≤200 m with $\log D_{TAC} = 2.40$; see also Table S2a).

It has been shown that HS are resolved by the SA method of CLE-AdCSV (Abualhaija & van den Berg, 2014; Mahmood et al., 2015). Earlier work indicated that CLE-AdCSV using SA would be more suitable to detect weaker binding HS, whereas TAC is the stronger AL and therefore less able to establish a competitive equilibrium with HS (Gledhill, 2012; Laglera et al., 2011). Direct addition of the SRFA standard to a TAC-analyzed sample did not result in any change in $[L_t]_{TAC}$ (Laglera et al., 2011; Slagter et al., 2017; Figures S2a and S2c). TAC itself may interact with HS, which limits formation of the $FeTAC_2$ complex and obfuscates its competition with Fe-binding organic ligands in the sample (Laglera et al., 2011). Furthermore, where a stark difference is observed across the TPD influence, $\log K'_{Fe'L}$ does not reflect this (Table 1). However, this is true for both the TAC and SA methods in this study. From the present data it cannot be

concluded whether TAC misses a specific ligand group or that a threshold value exists below which TAC cannot detect HS, possibly because of an interference between TAC and HS as suggested by Laglera et al. (2011). It is currently unclear by which mechanism the TAC method fails to detect HS. However, we do know that this is probably not due to simple outcompetition of HS by TAC, since the detection window of TAC, as applied here, and the maximum reactivity of the natural ligands (α_{FeHS}) are not very different from each other ($\log D_{TAC} = 2.4$, $\log\alpha_{FeHS} = 2.03$).

Attributing the greater Fe-binding organic ligand concentrations found by the SA method to the ability of resolving the iron binding properties of HS alone is proven wrong here, as the representation of the Fe-binding organic ligand pool by either method is more nuanced. For one, increases in $[L_t]_{TAC}$ are observed in the humic-rich Arctic surface samples. While lower than $[L_t]_{SA}$, the increase in $[L_t]_{TAC}$ strongly correlates with HS descriptors (Slagter et al., 2017) and direct voltammetric measurements of HS with SRFA as a humic representative standard (Dulaquais et al., 2018; this study). While ligand saturation is found using the TAC method, which suggests that part of the ligand pool is not measured, which in turn is further cemented by the lack of response upon addition of SRFA (Figure S2), we do show that TAC reflects at least part of the HS. TAC has been used successfully to relate HS to Fe-binding organic ligand concentrations on several occasions (Dulaquais et al., 2018; Slagter et al., 2017). However, this work calls into question if the entire contribution of HS to the complexing capacities reported was accounted for in those previous works.

In summary, it is not as simple as to describe one of the CLE-AdCSV methods here employed as superior for the elucidation of Fe-binding organic ligands in the Arctic Ocean specifically. Given the similar detection windows for either CLE-AdCSV method, we should not expect differences in ligand classes detected. Both CLE-AdCSV methods have their issues, and the HS standard in common use is not representative for the local HS pool. However, the analysis using SA has provided more insight in the Fe-binding organic ligand pool in the Arctic Ocean by widening the array of substances reflected. Going forward, it is recommended to use multiple methods. More knowledge about the relative differences between methods, such as the pH and equilibration time that can be used, is required before a definitive recommendation can be made. However, in areas where HS are important, we can recommend avoiding the TAC method.

4.3. Arctic Fe Speciation

Stations inside the TPD influence area show an increase in DFe and Fe-binding organic ligands along with HS representative measurements such as [HS] and FDOM. When measured using the TAC method previously (Slagter et al., 2017), these higher concentrations have been found to correlate significantly to known descriptors of riverine influences and HS in particular. Notably, however, at stations 99 and 125 the $[L_t]_{TAC}$ was lower than DFe for four and three samples inside the TPD, respectively (Figures 2d and 2f), suggesting that there are insufficient ligands to bind Fe and thus explain DFe. In contrast, $[L_t]_{SA}$ is higher than DFe in all samples, explaining the high Fe solubility in the TPD. The good correlation between HS and DFe indicates that HS is responsible for this high solubility. The lack of sufficient Fe-binding organic ligands measured using the TAC method has here been shown to be due to a methodical limitation. This is especially essential inside the TPD flow area and is reflected in a strong difference in L'_{TAC}/L'_{SA} (Table 2).

A near 1:1 ratio as found for $[L_t]_{HS}$ versus $[L_t]_{TAC}$ inside the TPD (Figure 6b) can be interpreted as an indication that the Fe-binding organic ligands inside the TPD are HS. Furthermore, recent analysis in TPD waters of the voltammetric response of Fe-HS complexes without altering DFe has shown that iron speciation is dominated by the formation of complexes with HS (Sukekava et al., 2018). It then stands to reason that Fe-binding organic ligands outside the TPD are of different origins, such as sea ice melt, marine biota, and even marine humics. Hence, we can now say that indeed all of the increased DFe transported across the Arctic Ocean (Rijkenberg et al., 2018) is complexed and predominantly by HS. This DFe, and the HS it is mobilized by, is introduced into the Arctic Ocean via the major rivers surrounding it, increasing the potential for primary production. This enrichment is contained to the TPD (Table 2), and prior study has already shown that outside the TPD Fe limitation already occurs in the surface waters over the Nansen Basin (Rijkenberg et al., 2018). In a future Arctic Ocean, subject to lesser sea ice extent and therefore a higher light availability and increased primary production (Arrigo & Van Dijken, 2011; Bhatt et al., 2014; Vancoppenolle et al., 2013), Fe-limitation is expected to become more important and the difference in DFe and Fe-binding organic ligands between surface waters inside and outside the

flow path of the TPD will be exacerbated. In the TPD changes are also expected to occur, with increasing river runoff and an increase in organic load of this runoff due to loss of permafrost in the catchment areas of these rivers already observed (Frey & McClelland, 2009; Vonk et al., 2012). Therefore, the entire Fe biogeochemistry, in terms of DFe, speciation, and bioavailability, of the Arctic Ocean may be further diversified across the boundary of the TPD.

The difference between $[L_t]_{TAC}$ and $[L_t]_{SA}$ is more pronounced inside the TPD but still presents outside the TPD, whereas $\log K'_{Fe'L}$ inside and outside of the TPD does not vary. Little variation in $\log K'_{Fe'L}$ was also found by others using both methods. Abualhaija et al. (2015) using SA found $11.1 \leq \log K'_{Fe'L} \leq 11.3$ in the Irish Sea. In the Atlantic Ocean Batchelli et al. (2010) using TAC put $\log K'_{Fe'L}$ between 11.8 and 12.0, whereas in the Mediterranean Sea Gerringa et al. (2017), also using TAC, found $\log K'_{Fe'L}$ values averaged per water depth between 11.6 and 12.13. Mahmood et al. (2015) observed larger variation with an average range of $10.6 \leq \log K'_{Fe'L} \leq 12.7$ in the Irish Sea. In the present study $\log K'_{Fe'L}$ values of both methods fell within those found in the quoted studies (Table 1).

Our results do not show a decrease in $\log K'_{Fe'L}$ when comparing samples outside the TPD with samples inside the TPD, for both methods. This result contradicts the supposition that HS have a relatively low binding constant with Fe. The TAC-derived $\log K'_{Fe'L}$ in the Barents Sea was the same as the samples in the open Arctic Ocean. In contrast, the SA-derived $\log K'_{Fe'L}$ was lower in the Barents Sea than in the open Arctic Ocean stations and the only significantly lower $\log K'_{Fe'L}$ in comparison to TAC. Two ligand classes could be resolved in more cases for measurements using SA than for TAC. This discrepancy was particularly clear at 30–200 m at stations 69, 99, 101, and 125 (see also Figure S1 and Tables S2a and S2b). Their distinction is based on K′ with, looking at both methods, a strong L_1 class ranging $12.6 \leq \log K'_{Fe'L} \leq 14.5$ taking standard deviations into account and a weaker L_2 class ranging $10.2 \leq \log K'_{Fe'L} \leq 11.4$. The above $\log K'_{Fe'L}$ ranges for L_2 have been connected to estuarine outflow and HS (Bundy et al., 2015; Gledhill, 2012). However, both $L_{1,SA}$ and $L_{2,SA}$ contribute to the increases we observe in $[L_t]$ inside the TPD and thus with HS. Therefore, HS are not only part of the weaker L_2 but also correlate with the stronger L_1. Although the more inclusive two-ligand determination using SA results in $\log K'_{Fe'L}$ ranges that are not atypical for the region studied, the lack of resolution and confidence in $\log K'_{Fe'L}$ (see section 4.1) must be kept in mind.

The sum of both ligand classes in the two-ligand model for SA ($\Sigma_{L1,L2;SA}$) agreed very well with $[L_t]_{SA}$. Therefore, the concentrations of Fe-binding organic ligands are probably good, but as per the prior paragraph, K′ may be imprecise. There was a marked difference between $\Sigma_{L1,L2;TAC}$ and $[L_t]_{TAC}$, with the sum of the separate ligand groups being higher (Figures 2a–2c and 3a and 3b). $\Sigma_{L1,L2;TAC}$ may explain the presence of the high DFe in the uppermost samples where these concentrations are not explained by $[L_t]_{TAC}$. However, the disagreement between $[L_t]_{TAC}$ and $\Sigma_{L1,L2;TAC}$ also indicates a troublesome fit of the two-ligand Langmuir model, hampering data quality in this respect. Ostensibly, there is an issue measuring HS using TAC, as oversaturation of ligands is not likely to persist if it occurs and L_t and $\Sigma_{L1,L2}$ need to agree. These issues do not occur for measurements using SA. TAC not reflecting all HS is the most probable explanation, as revisited in the next section. We can conclude that the ligand concentrations of the two ligand groups obtained with SA are probably correct, whereas those of TAC might have a larger error. It is the relative weak ligand determined by SA that is elevated in the TPD surface waters. However, because the strong ligand obtained by the SA method falls outside the detection window the $\log K'_{Fe'L}$ values may be imprecise.

5. Conclusions

Analyses with SA as a competitive ligand were performed on select samples coinciding with analyses using TAC by (Slagter et al., 2017). Additionally, measurements of [HS] were performed. $[L_t]_{SA}$ was higher overall, but especially inside the TPD, and explained the existence of high DFe above the solubility product of inorganic Fe-oxy (hydr)oxides. Still both CLE-AdCSV methods clearly show correlation with this TPD influence, which in turn is well described by HS properties including a representative $[L_t]_{HS}$ derived from the binding capacity of the SRFA standard used.

Both CLE-AdCSV methods have a ratio near 1 with $[L_t]_{HS}$, with an offset to higher concentrations for $[L_t]_{SA}$. While an $[L_t]_{HS}/[L_t]_{TAC}$ ratio near 1 could be seen as suggestive of domination of the Fe-binding organic ligand pool by HS, the occurrence of ligand saturation in TAC measurements, which is

thermodynamically improbable, indicates that part of the (humic) ligand pool remains veiled using the TAC method. The offset between both methods does remain outside the TPD but decreases. Here $[L_t]_{SA}$ decreases with $[L_t]_{HS}$, whereas $[L_t]_{TAC}$ does not, possibly due to a different origin of the (humic) ligands. Additionally, our results and the lack of response of CLE-AdCSV using TAC to addition of the SRFA standard further confirm that TAC cannot resolve part of HS.

Differences in $[L_t]$ using either method or correlation to HS are not reflected in K′, making it very difficult to recognize the contribution of HS by ligand class. Analysis using SA can be resolved for two ligand groups for more samples, again especially for surface samples. In samples where two ligand groups can be resolved using both methods, $\log K_1'_{Fe'L(SA)}$ agrees reasonably with $\log K_1'_{Fe'L(TAC)}$ and therefore presumably describes the same ligand group. $\log K_2'_{Fe'L(SA)}$ is weaker than $\log K_2'_{Fe'L(TAC)}$, indicating a disparity in the ligands.

The HS carried across the Arctic Ocean surface by the TPD are responsible for the transport of DFe. The Arctic today is subject to rapid loss of permafrost, releasing many complex organics into the rivers (Frey & McClelland, 2009), a signal already proven to reach well into the shelf seas (Vonk et al., 2012), adding to the (C)DOM pool transported by the TPD and DFe and HS to bind it. Issues with TAC′s ability to resolve certain HS lead to TAC only reflecting 61% of $[L_t]_{SA}$. Issues with SA equilibration may lead to an overestimation of $[L_t]$. In conclusion, comparison between methods brings a more complex relation to light and suggests that method intercalibration in the presence of a variety of model ligands, multiple methods, detection windows, and equilibration times may be required to properly ascertain the overall organic Fe-binding organic ligand pool in natural seawater samples.

Acknowledgments
This research was funded by the Netherlands Organisation for Scientific Research (NWO) under project 822.01.018 to L. J. A. Gerringa. C. Sukekava was funded by the Beca Santander Iberoamerica program. We are indebted to GEOTRACES for the opportunity to take part in the PS94 expedition on FS Polarstern, in which captain and crew offered excellent logistical support. Furthermore, we thank P. I. Ursula Schauer, the ultraclean team (Micha Rijkenberg, Aridane Gonzalez, Lars-Eric Heimburger, Michael Staubwasser, and Sven Ober) for their scientific support. We thank Martin Laan and Sander Asjes (NIOZ Marine Technology) for their modification of our voltammetric equipment for atmospheric purging. We are indebted to students David Amptmeijer, Robert Sluijter, and Ismaël Salazar, who have performed many measurements to arrive at the present data set. We are grateful for the comments of anonymous reviewers that improved the manuscript considerably. Upon acceptance of the manuscript, the data will be made accessible in Pangaea (https://www.pangaea.de) and with the BODC (http://www.bodc.ac.uk/geotraces).

References

Abualhaija, M. M., & van den Berg, C. M. G. (2014). Chemical speciation of iron in seawater using catalytic cathodic stripping voltammetry with ligand competition against salicylaldoxime. *Marine Chemistry*, *164*, 60–74. https://doi.org/10.1016/j.marchem.2014.06.005

Abualhaija, M. M., Whitby, H., & van den Berg, C. M. G. (2015). Competition between copper and iron for humic ligands in estuarine waters. *Marine Chemistry*, *172*, 46–56. https://doi.org/10.1016/j.marchem.2015.03.010

Amon, R. M. W., Gereon, B., & Benedikt, M. (2003). Dissolved organic carbon distribution and origin in the Nordic Seas: Exchanges with the Arctic Ocean and the North Atlantic. *Journal of Geophysical Research*, *108*, 3221. https://doi.org/10.1029/2002JC001594

Apte, S. C., Gardner, M. J., & Ravenscroft, J. E. (1988). An evaluation of voltammetric titration procedures for the determination of trace metal complexation in natural waters by use of computers simulation. *Analytica Chimica Acta*, *212*, 1–21. https://doi.org/10.1016/S0003-2670(00)84124-0

Arrigo, K. R., & van Dijken, G. L. (2011). Secular trends in Arctic Ocean net primary production. *Journal of Geophysical Research, Oceans*, *116*, C09011. https://doi.org/10.1029/2011JC007151

Batchelli, S., Muller, F. L. L., Chang, K. C., & Lee, C. L. (2010). Evidence for strong but dynamic iron-humic colloidal associations in humic-rich coastal waters. *Environmental Science and Technology*, *44*(22), 8485–8490. https://doi.org/10.1021/es101081c

Benner, R., Louchouarn, P., & Amon, R. M. W. (2005). Terrigenous dissolved organic matter in the Arctic Ocean and its transport to surface and deep waters of the North Atlantic. *Global Biogeochemical Cycles*, *19*, GB2025. https://doi.org/10.1029/2004GB002398

Bhatt, U. S., Walker, D. A., Walsh, J. E., Carmack, E. C., Frey, K. E., Meier, W. N., et al. (2014). Implications of Arctic sea ice decline for the Earth system. *Annual Review of Environment and Resources*, *39*(1), 57–89. https://doi.org/10.1146/annurev-environ-122012-094357

Boiteau, R. M., Mende, D. R., Hawco, N. J., McIlvin, M. R., Fitzsimmons, J. N., Saito, M. A., et al. (2016). Siderophore-based microbial adaptations to iron scarcity across the eastern Pacific Ocean. *Proceedings of the National Academy of Sciences*, *113*(50), 14,237–14,242. https://doi.org/10.1073/pnas.1608594113

Boyd, P. W., Arrigo, K. R., Strzepek, R., & van Dijken, G. L. (2012). Mapping phytoplankton iron utilization: Insights into Southern Ocean supply mechanisms. *Journal of Geophysical Research*, *117*, C06009. https://doi.org/10.1029/2011JC007726

Bronk, D. A. (2002). Dynamics of DON. In D. A. Hansell & C. A. Carlson (Eds.), *Biogeochemistry of marine dissolved organic matter* (pp. 153–247). London: Academic Press.

Buck, K. N., Gerringa, L. J. A., & Rijkenberg, M. J. A. (2016). An intercomparison of dissolved iron speciation at the Bermuda Atlantic Time-series Study (BATS) site: Results from GEOTRACES crossover station A. *Frontiers in Marine Science*, *3*, 262. https://doi.org/10.3389/fmars.2016.00262

Buck, K. N., Lohan, M. C., Berger, C. J. M., & Bruland, K. W. (2007). Dissolved iron speciation in two distinct river plumes and an estuary: Implications for riverine iron supply. *Limnology and Oceanography*, *52*(2), 843–855. https://doi.org/10.4319/lo.2007.52.2.0843

Buck, K. N., Moffett, J., Barbeau, K. A., Bundy, R. M., Kondo, Y., & Wu, J. (2012). The organic complexation of iron and copper: An intercomparison of competitive ligand exchange-adsorptive cathodic stripping voltammetry (CLE-ACSV) techniques. *Limnology and Oceanography: Methods*, *10*(7), 496–515. https://doi.org/10.4319/lom.2012.10.496

Buffle, J. (1988). *Complexation reactions in aquatic systems: An analytical approach* (1st ed.). Chichester, UK: Ellis Horwood.

Buffle, J. (1990). The analytical challenge posed by fulvic and humic compounds. *Analytica Chimica Acta*, *232*, 1–2. https://doi.org/10.1016/S0003-2670(00)81219-2

Bundy, R. M., Abdulla, H. A. N., Hatcher, P. G., Biller, D. V., Buck, K. N., & Barbeau, K. A. (2015). Iron-binding ligands and humic substances in the San Francisco Bay estuary and estuarine-influenced shelf regions of coastal California. *Marine Chemistry*, *173*, 183–194. https://doi.org/10.1016/j.marchem.2014.11.005

Bundy, R. M., Boiteau, R. M., McLean, C., Turk-Kubo, K. A., McIlvin, M. R., Saito, M. A., et al. (2018). Distinct siderophores contribute to iron cycling in the mesopelagic at station ALOHA. *Frontiers in Marine Science*, *5*, 1–15. https://doi.org/10.3389/fmars.2018.00061

Coble, P. G. (2007). Marine optical biogeochemistry: The chemistry of ocean color. *Chemical Reviews*, *107*(2), 402–418. https://doi.org/10.1021/cr050350+

Croot, P. L., & Johansson, M. (2000). Determination of iron speciation by cathodic stripping voltammetry in seawater using the competing ligand 2-(2-thiazolylazo)-p-cresol (TAC). *Electroanalysis*, *12*(8), 565–576. https://doi.org/10.1002/(SICI)1521-4109(200005)12:8<565::AID-ELAN565>3.0.CO;2-L

van den Berg, C. M. G. (2006). Chemical speciation of iron in seawater by cathodic stripping voltammetry with dihydroxynaphthalene. *Analytical Chemistry*, *78*(1), 156–163. https://doi.org/10.1021/ac051441+

van den Berg, C. M. G., Nimmo, M., Daly, P., & Turner, D. R. (1990). Effects of the detection window on the determination of organic copper speciation in estuarine waters. *Analytica Chimica Acta*, *232*, 149–159. https://doi.org/10.1016/S0003-2670(00)81231-3

Dulaquais, G., Waeles, M., Gerringa, L. J. A., Middag, R., Rijkenberg, M. J. A., & Riso, R. (2018). The biogeochemistry of electroactive humic substances and its connection to iron chemistry in the North East Atlantic and the Western Mediterranean Sea. *Journal of Geophysical Research: Oceans*, *123*, 5481–5499. https://doi.org/10.1029/2018JC014211

Frey, K. E., & McClelland, J. W. (2009). Impacts of permafrost degradation on arctic river biogeochemistry. *Hydrological Processes*, *23*(1), 169–182. https://doi.org/10.1002/hyp.7196

Geider, R. J., & La Roche, J. (1994). The role of iron in phytoplankton photosynthesis, and the potential for iron-limitation of primary productivity in the sea. *Photosynthesis Research*, *39*(3), 275–301. https://doi.org/10.1007/BF00014588

Gerringa, L. J. A., Rijkenberg, M. J. A., Thuróczy, C. E., & Maas, L. R. M. (2014). A critical look at the calculation of the binding characteristics and concentration of iron complexing ligands in seawater with suggested improvements. *Environmental Chemistry*, *11*(2), 114–136. https://doi.org/10.1071/EN13072

Gerringa, L. J. A., Slagter, H. A., Bown, J., van Haren, H., Laan, P., de Baar, H. J. W., & Rijkenberg, M. J. A. (2017). Dissolved Fe and Fe-binding organic ligands in the Mediterranean Sea—GEOTRACES G04. *Marine Chemistry*, *194*, 100–113. https://doi.org/10.1016/j.marchem.2017.05.012

Gledhill, M. (2012). The organic complexation of iron in the marine environment: A review. *Frontiers in Microbiology*, *3*. https://doi.org/10.3389/fmicb.2012.00069

Gledhill, M., & Gerringa, L. J. A. (2017). The effect of metal concentration on the parameters derived from complexometric titrations of trace elements in seawater—A model study. *Frontiers in Marine Science*, *4*. https://doi.org/10.3389/fmars.2017.00254

Gledhill, M., McCormack, P., Ussher, S., Achterberg, E. P., Mantoura, R. F. C., & Worsfold, P. J. (2004). Production of siderophore type chelates by mixed bacterioplankton populations in nutrient enriched seawater incubations. *Marine Chemistry*, *88*(1–2), 75–83. https://doi.org/10.1016/j.marchem.2004.03.003

Gledhill, M., & van den Berg, C. M. G. (1994). Determination of complexation of iron (III) with natural organic complexing ligands in seawater using cathodic stripping voltammetry. *Marine Chemistry*, *47*(1), 41–54. https://doi.org/10.1016/0304-4203(94)90012-4

Gordienko, P. A., & Laktionov, A. F. (1969). Circulation and physics of the Arctic basin waters. In A. L. Gordon & F. W. G. Baker (Eds.), *Oceanography: Annals of the international geophysical year* (Vol. 46, pp. 94–112). London: Pergamon Press.

Gregor, D. J., Loeng, H., & Barrie, L. (1998). The influence of physical and chemical processes on contaminant transport into and within the Arctic. Arctic Monitoring and Assessment Report*:* Arctic Pollution Issues.

Guéguen, C., Guo, L., Yamamoto-Kawai, M., & Tanaka, N. (2007). Colored dissolved organic matter dynamics across the shelf-basin interface in the western Arctic Ocean. *Journal of Geophysical Research, Oceans*, *112*, C07031. https://doi.org/10.1029/2006JC003584

Hassler, C. S., Schoemann, V., Nichols, C. M., Butler, E. C. V., & Boyd, P. W. (2011). Saccharides enhance iron bioavailability to Southern Ocean phytoplankton. *Proceedings of the National Academy of Sciences of the United States of America*, *108*(3), 1076–1081. https://doi.org/10.1073/pnas.1010963108

Hassler, C. S., van den Berg, C. M. G., & Boyd, P. W. (2017). Toward a regional classification to provide a more inclusive examination of the ocean biogeochemistry of iron-binding ligands. *Frontiers in Marine Science*, *4*(February), 19. https://doi.org/10.3389/fmars.2017.00019

Hioki, N., Kuma, K., Morita, Y., Sasayama, R., Ooki, A., Kondo, Y., et al. (2014). Laterally spreading iron, humic-like dissolved organic matter and nutrients in cold, dense subsurface water of the Arctic Ocean. *Scientific Reports*, *4*, 1–9. https://doi.org/10.1038/srep06775

Intergovernmental Panel on Climate Change. (2014). Climate change 2014: Synthesis report. Contribution of Working Groups I, II and III to the Fifth Assessment Report of the Intergovernmental Panel on Climate Change. (Core Writing Team, L. A. Meyer, & R. K. Pachauri, Eds.). Geneva, Switzerland: IPCC. Retrieved from https://www.ipcc.ch/report/ar5/syr/, https://doi.org/10.1586/17446651.2014.934607

Krachler, R., Krachler, R. F., Wallner, G., Hann, S., Laux, M., Cervantes Recalde, M. F., et al. (2015). River-derived humic substances as iron chelators in seawater. *Marine Chemistry*, *174*, 85–93. https://doi.org/10.1016/j.marchem.2015.05.009

Laglera, L. M., Battaglia, G., & van den Berg, C. M. G. (2007). Determination of humic substances in natural waters by cathodic stripping voltammetry of their complexes with iron. *Analytica Chimica Acta*, *599*(1), 58–66. https://doi.org/10.1016/j.aca.2007.07.059

Laglera, L. M., Battaglia, G., & van den Berg, C. M. G. (2011). Effect of humic substances on the iron speciation in natural waters by CLE/CSV. *Marine Chemistry*, *127*(1–4), 134–143. https://doi.org/10.1016/j.marchem.2011.09.003

Laglera, L. M., & Filella, M. (2015). The relevance of ligand exchange kinetics in the measurement of iron speciation by CLE–AdCSV in seawater. *Marine Chemistry*, *173*, 100–113. https://doi.org/10.1016/j.marchem.2014.09.005

Laglera, L. M., Santos-Echeandía, J., Caprara, S., & Monticelli, D. (2013). Quantification of iron in seawater at the low picomolar range based on optimization of bromate/ammonia/dihydroxynaphtalene system by catalytic adsorptive cathodic stripping voltammetry. *Analytical Chemistry*, *85*(4), 2486–2492. https://doi.org/10.1021/ac303621q

Laglera, L. M., & van den Berg, C. M. G. (2009). Evidence for geochemical control of iron by humic substances in seawater. *Limnology and Oceanography*, *54*(2), 610–619. https://doi.org/10.4319/lo.2009.54.2.0610

Liu, X., & Millero, F. J. (2002). The solubility of iron in seawater. *Marine Chemistry*, *77*(1), 43–54. https://doi.org/10.1016/S0304-4203(01)00074-3

Macdonald, R. W., Harner, T., & Fyfe, J. (2005). Recent climate change in the Arctic and its impact on contaminant pathways and interpretation of temporal trend data. *Science of the Total Environment*, *342*(1–3), 5–86. https://doi.org/10.1016/j.scitotenv.2004.12.059

Mahmood, A., Abualhaija, M. M., van den Berg, C. M. G., & Sander, S. G. (2015). Organic speciation of dissolved iron in estuarine and coastal waters at multiple analytical windows. *Marine Chemistry*, *177*, 706–719. https://doi.org/10.1016/j.marchem.2015.11.001

Millero, F. J. (1998). Solubility of Fe (III) in seawater. *Earth and Planetary Science Letters*, *154*, 323–329. https://doi.org/10.1016/S0012-821X(97)00179-9

Nakayama, Y., Fujita, S., Kuma, K., & Shimada, K. (2011). Iron and humic-type fluorescent dissolved organic matter in the Chukchi Sea and Canada Basin of the western Arctic Ocean. *Journal of Geophysical Research, Oceans*, *116*, C07031. https://doi.org/10.1029/2010JC006779

Netz, D. J. A., Stith, C. M., Stümpfig, M., Köpf, G., Vogel, D., Genau, H. M., et al. (2012). Eukaryotic DNA polymerases require an iron-sulfur cluster for the formation of active complexes. *Nature Chemical Biology*, *8*(1), 125–132. https://doi.org/10.1038/nchembio.721

Obernosterer, I., & Herndl, G. J. (2000). Differences in the optical and biological reactivity of the humic and nonhumic dissolved organic carbon component in two contrasting coastal marine environments. *Limnology and Oceanography*, *45*(5), 1120–1129. https://doi.org/10.4319/lo.2000.45.5.1120

Pernet-Coudrier, B., Waeles, M., Filella, M., Quentel, F., & Riso, R. D. (2013). Simple and simultaneous determination of glutathione, thioacetamide and refractory organic matter in natural waters by DP-CSV. *Science of the Total Environment*, *463-464*, 997–1005. https://doi.org/10.1016/j.scitotenv.2013.06.053

Press, W. H., Teukolsky, S. A., Vetterling, W. T., & Flannery, B. P. (2007). *Numerical recipes: The art of scientific computing* (3rd ed.). Cambridge, UK: Cambridge University Press. https://doi.org/10.1158/1078-0432.CCR-07-1112

Quentel, F., & Filella, M. (2008). Quantification of refractory organic substances in freshwaters: Further insight into the response of the voltammetric method. *Analytical and Bioanalytical Chemistry*, *392*(6), 1225–1230. https://doi.org/10.1007/s00216-008-2366-4

R Development Core Team (2008). *R: A language and environment for statistical computing*. Vienna, Austria: R Foundation for Statistical Computing. https://doi.org/10.1094/PDIS-92-11-1586C

Rabe, B., Schauer, U., Ober, S., Horn, M., Hoppmann, M., Korhonen, M., et al. (2016). Physical oceanography during POLARSTERN cruise PS94 (ARK-XXIX/3). Bremerhaven. https://doi.org/10.1594/PANGAEA.859558

Raiswell, R., & Anderson, T. F. (2005). Reactive iron enrichment in sediments deposited beneath euxinic bottom waters: Constraints on supply by shelf recycling. *Geological Society, London, Special Publications*, *248*(1), 179–194. https://doi.org/10.1144/GSL.SP.2005.248.01.10

Rijkenberg, M. J. A., Slagter, H. A., Rutgers van der Loeff, M., van Ooijen, J., & Gerringa, L. J. A. (2018). Dissolved Fe in the deep and upper Arctic Ocean with a focus on Fe limitation in the Nansen Basin. *Frontiers in Marine Science*, *5*, 1–14. https://doi.org/10.3389/fmars.2018.00088

Rudels, B. (2012). Arctic Ocean circulation and variability—Advection and external forcing encounter constraints and local processes. *Ocean Science*, *8*(2), 261–286. https://doi.org/10.5194/os-8-261-2012

Rue, E. L., & Bruland, K. W. (1995). Complexation of iron (III) by natural organic ligands in the Central North Pacific as determined by a new competitive ligand equilibration/adsorptive cathodic stripping voltammetric method. *Marine Chemistry*, *50*(1–4), 117–138. https://doi.org/10.1016/0304-4203(95)00031-L

Rutgers van der Loeff, M., Cai, P., Stimac, I., Bauch, D., Hanfland, C., Roeske, T., & Moran, S. B. (2012). Shelf-basin exchange times of Arctic surface waters estimated from ^{228}Th/^{228}Ra disequilibrium. *Journal of Geophysical Research, Oceans*, *117*, C03024. https://doi.org/10.1029/2011JC007478

Schuur, E. A. G., McGuire, A. D., Schädel, C., Grosse, G., Harden, J. W., Hayes, D. J., et al. (2015). Climate change and the permafrost carbon feedback. *Nature*, *520*(7546), 171–179. https://doi.org/10.1038/nature14338.

Slagter, H. A., Reader, H. E., Rijkenberg, M. J. A., Rutgers van der Loeff, M., de Baar, H. J. W., & Gerringa, L. J. A. (2017). Organic Fe speciation in the Eurasian Basins of the Arctic Ocean and its relation to terrestrial DOM. *Marine Chemistry*, *197*, 11–25. https://doi.org/10.1016/j.marchem.2017.10.005

Strzepek, R. F., Maldonado, M. T., Hunter, K. A., Frew, R. D., & Boyd, P. W. (2011). Adaptive strategies by Southern Ocean phytoplankton to lessen iron limitation: Uptake of organically complexed iron and reduced cellular iron requirements. *Limnology and Oceanography*, *56*(6), 1983–2002. https://doi.org/10.4319/lo.2011.56.6.1983

Sukekava, C., Downes, J., Slagter, H. A., Gerringa, L. J. A., & Laglera, L. M. (2018). Determination of the contribution of humic substances to iron complexation in seawater by catalytic cathodic stripping voltammetry. *Talanta*, *189*, 359–364. https://doi.org/10.1016/j.talanta.2018.07.021

Sunda, W., & Huntsman, S. (2003). Effect of pH, light, and temperature on Fe–EDTA chelation and Fe hydrolysis in seawater. *Marine Chemistry*, *84*(1–2), 35–47. https://doi.org/10.1016/s0304-4203(03)00101-4

Timmermans, K. R., Davey, M. S., van der Wagt, B., Snoek, J., Geider, R. J., Veldhuis, M. J. W., et al. (2001). Co-limitation by iron and light of Chaetoceros brevis, C. dichaeta and C. calcitrans (Bacillariophyceae). *Marine Ecology Progress Series*, *217*, 287–297. https://doi.org/10.3354/meps217287

Timmermans, K. R., Gerringa, L. J. A., de Baar, H. J. W., van der Wagt, B., Veldhuis, M. J. W., de Jong, J. T. M., et al. (2001). Growth rates of large and small Southern Ocean diatoms in relation to availability of iron in natural seawater. *Limnology and Oceanography*, *46*(2), 260–266. https://doi.org/10.4319/lo.2001.46.2.0260

Vancoppenolle, M., Bopp, L., Madec, G., Dunne, J., Ilyina, T., Halloran, P. R., & Steiner, N. (2013). Future arctic ocean primary productivity from CMIP5 simulations: Uncertain outcome, but consistent mechanisms. *Global Biogeochemical Cycles*, *27*, 605–619. https://doi.org/10.1002/gbc.20055

Velasquez, I., Nunn, B. L., Ibisanmi, E., Goodlett, D. R., Hunter, K. A., & Sander, S. G. (2011). Detection of hydroxamate siderophores in coastal and sub-Antarctic waters off the South Eastern Coast of New Zealand. *Marine Chemistry*, *126*(1–4), 97–107. https://doi.org/10.1016/j.marchem.2011.04.003

Velasquez, I. B., Ibisanmi, E., Maas, E. W., Boyd, P. W., Nodder, S., & Sander, S. G. (2016). Ferrioxamine siderophores detected amongst iron binding ligands produced during the remineralization of marine particles. *Frontiers in Marine Science*, *3*. https://doi.org/10.3389/fmars.2016.00172

Vonk, J. E., Mann, P. J., Davydov, S., Davydova, A., Spencer, R. G. M., Schade, J., et al. (2013). High biolability of ancient permafrost carbon upon thaw. *Geophysical Research Letters*, *40*, 2689–2693. https://doi.org/10.1002/grl.50348

Vonk, J. E., Sánchez-García, L., van Dongen, B. E., Alling, V., Kosmach, D., Charkin, A., et al. (2012). Activation of old carbon by erosion of coastal and subsea permafrost in Arctic Siberia. *Nature*, *489*(7414), 137–140. https://doi.org/10.1038/nature11392

Wilhelm, S. W., King, A. L., Twining, B. S., LeCleir, G. R., DeBruyn, J. M., Strzepek, R. F., et al. (2013). Elemental quotas and physiology of a southwestern Pacific Ocean plankton community as a function of iron availability. *Aquatic Microbial Ecology*, *68*(3), 185–194. https://doi.org/10.3354/ame01611

Zhang, C. (2014). Essential functions of iron-requiring proteins in DNA replication, repair and cell cycle control. *Protein & Cell*, *5*(10), 750–760. https://doi.org/10.1007/s13238-014-0083-7